

Manipulating quantum materials with quantum light

Martin Kiffner^{1,2}, Jonathan R. Coulthard², Frank Schlawin², Arzhang Ardavan², and Dieter Jaksch^{2,1}
*Centre for Quantum Technologies, National University of Singapore, 3 Science Drive 2, Singapore 117543¹ and
Clarendon Laboratory, University of Oxford, Parks Road, Oxford OX1 3PU, United Kingdom²*

We show that the macroscopic magnetic and electronic properties of strongly correlated electron systems can be manipulated by coupling them to a cavity mode. As a paradigmatic example we consider the Fermi-Hubbard model and find that the electron-cavity coupling enhances the magnetic interaction between the electron spins in the ground-state manifold. At half filling this effect can be observed by a change in the magnetic susceptibility. At less than half filling, the cavity introduces a next-nearest neighbour hopping and mediates a long-range electron-electron interaction between distant sites. We study the ground state properties with Tensor Network methods and find that the cavity coupling can induce a new phase characterized by a momentum-space pairing effect for electrons.

I. INTRODUCTION

The ability to control and manipulate complex quantum systems is of paramount importance for future quantum technologies. Of particular interest are quantum hybrid systems [1, 2] where different quantum objects hybridize to exhibit properties not shared by the individual components. Examples of this hybridization effect in cold atom systems coupled to optical cavities are given by self-organization phenomena [3–7] as well as the occurrence of quantum phase transitions and exotic quantum phases [8–11].

Recently, the class of available hybrid systems has been extended by solid state systems that couple strongly to microwave, terahertz or optical radiation [12–30]. For example, the coupling of microwave cavities to magnon and spinon excitations in magnetic materials has been investigated in [12–16] and [17], respectively. Two-dimensional electron gases in magnetic fields can couple very strongly to terahertz cavities [18–20] such that Bloch-Siegert shifts become observable [21], and tomography of an ultra-strongly coupled polariton state was presented in [22] using magneto-transport measurements [23]. A recent experiment [24] has demonstrated that coupling of an organic semiconductor to an optical cavity enhances the electric conductivity, which can be understood in terms of delocalized exciton polaritons [25, 26].

A special class of solid state systems are quantum materials [31–34] where small microscopic changes can result in large macroscopic responses due to strong electron-electron interactions. Coupling these systems to cavities opens up the fascinating possibility of investigating the ultimate quantum limit where macroscopic properties of quantum materials are determined by quantum light fields and vice versa. First steps into this direction have been undertaken recently [27–30, 35]. For example, quantum counterparts of light-induced superconductivity [36–39] have been investigated in [27–29, 35] using terahertz and microwave cavities, and a superradiant phase of a cavity-coupled quantum material has been predicted in [30].

Here we show that shaping the vacuum via a cavity

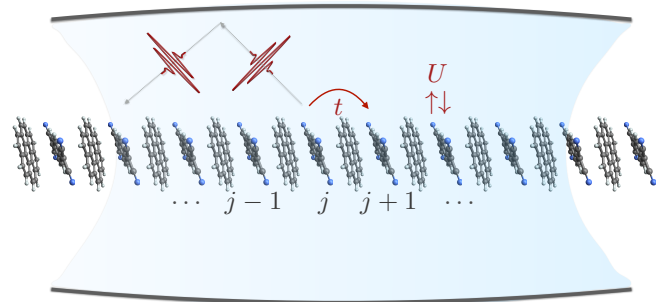


FIG. 1. (Color online) The system of interest is given by an electronic system coupled to a single-mode cavity. The electronic system is described by the Fermi-Hubbard model with on-site interaction U and hopping amplitude t between neighbouring sites.

allows one to manipulate macroscopic properties like the magnetic susceptibility of a quantum material. As a paradigmatic model of quantum materials we consider the Fermi-Hubbard model [40] which captures the interplay between kinetic fluctuations and strong, local, electron-electron interactions [32–34]. While the interaction of these systems with strong, classical light fields has been investigated, for example, in [41–44], the intriguing possibility of coupling them to quantum light fields has not been explored yet.

More specifically, we consider a one-dimensional Hubbard model coupled to a single mode of an empty cavity. For an electronic system at half filling we find that the electron-cavity interaction enhances the magnetic interactions between spins in the ground-state manifold. This effect can be experimentally observed by measuring the magnetic susceptibility.

At less than half filling, the cavity coupling introduces (i) a next-nearest neighbour hopping, (ii) an on-site energy shift and (iii) a long-range electron-electron interaction between distant sites. We investigate the ground state of the electronic system at less than half filling and in the presence of the cavity with density matrix renormalization group (DMRG) techniques [45, 46]. We

find that the cavity induces momentum-space pairing for mesoscopic electron systems. The transition to this new phase is a collectively enhanced effect and does not require ultra-strong coupling on the single-electron level and scales with $1/\sqrt{v_{\text{uc}}}$, where v_{uc} is the volume of the unit cell of the crystal.

This paper is organized as follows. In Sec. II we introduce our model for the system shown in Fig. 1. Our results are presented in Sec. III, and their experimental realization is discussed in Sec. IV. A brief discussion and conclusion is provided in Sec. V.

II. MODEL

The system shown in Fig. 1 is comprised of an electronic system coupled to a single-mode cavity. We introduce the Hamiltonian describing this quantum hybrid system in Sec. II A, and discuss its gross energy structure for the parameters of interest in Sec. II B.

A. System Hamiltonian

We begin with the description of the system Hamiltonian with the single-mode cavity with resonance frequency ω_c . The Hamiltonian for the cavity photons with energy $\Omega = \hbar\omega_c$ is

$$\hat{P} = \Omega \hat{a}^\dagger \hat{a}, \quad (1)$$

where \hat{a}^\dagger (\hat{a}) is the bosonic photon creation (annihilation) operator. The eigenstates of \hat{P} are the photon number states $|j_P\rangle$ with $\hat{P}|j_P\rangle = j\Omega|j_P\rangle$. The spectral decomposition of \hat{P} can thus be written as

$$\hat{P} = \Omega \sum_{j=0}^{\infty} j \hat{\mathcal{P}}_j^P, \quad (2)$$

where

$$\hat{\mathcal{P}}_j^P = |j_P\rangle\langle j_P| \quad (3)$$

is the projector onto the state with j photons.

The electronic system is described by the one-dimensional Fermi-Hubbard model [40] with Hamiltonian

$$\hat{H}_{\text{FH}} = \hat{T} + \hat{D}, \quad (4)$$

where

$$\hat{T} = -t \sum_{\langle jk \rangle \sigma} (\hat{c}_{j,\sigma}^\dagger \hat{c}_{k,\sigma} + \text{h.c.}) \quad (5)$$

accounts for hopping between neighbouring sites $\langle jk \rangle$ with $j < k$, t is the hopping amplitude and $\hat{c}_{j,\sigma}^\dagger$ ($\hat{c}_{j,\sigma}$) creates (annihilates) an electron at site j in spin state $\sigma \in \{\uparrow, \downarrow\}$. The second term in Eq. (4) describes the on-site Coulomb interaction between electrons,

$$\hat{D} = U \sum_j \hat{n}_{j,\uparrow} \hat{n}_{j,\downarrow}, \quad (6)$$

where U is the interaction energy and $\hat{n}_{j,\sigma} = \hat{c}_{j,\sigma}^\dagger \hat{c}_{j,\sigma}$ counts the number of electrons at site j in spin state σ . Each site can accommodate at most two electrons with opposite spins, and in the following we refer to doubly occupied sites as doublons.

The operator \hat{D} is diagonal in the basis of Wannier states [40],

$$|\mathbf{x}, \mathbf{s}\rangle = \hat{c}_{x_N, s_N}^\dagger \dots \hat{c}_{x_1, s_1}^\dagger |0_E\rangle, \quad (7)$$

where $|0_E\rangle$ is the vacuum state of the electronic system and

$$\mathbf{x} = (x_1, \dots, x_N), \quad (8a)$$

$$\mathbf{s} = (s_1, \dots, s_N), \quad (8b)$$

are row vectors with $x_j \in \{1, \dots, L\}$, $s_j \in \{\uparrow, \downarrow\}$ and $j \in \{1, \dots, N\}$. The vectors in Eq. (8) describe the spatial distribution of N electrons and their spin state in a one-dimensional lattice with L sites.

The Wannier states are eigenstates of \hat{D} and form degenerate manifolds with energies kU , where k is an integer that counts the total number of doubly occupied sites in $|\mathbf{x}, \mathbf{s}\rangle$. In the following we refer to doubly occupied sites as doublons. The projector onto the manifold with k doublons is given by [40]

$$\hat{\mathcal{P}}_k^D = \frac{(-1)^k}{k!} \partial_x^k G(x) \Big|_{x=1}, \quad (9)$$

where

$$G(x) = \prod_{j=1}^L (1 - x \hat{n}_{j,\uparrow} \hat{n}_{j,\downarrow}) \quad (10)$$

is the generating function. The spectral decomposition of \hat{D} is thus given by

$$\hat{D} = U \sum_{k=0}^L k \hat{\mathcal{P}}_k^D. \quad (11)$$

Note that in general, each manifold with a given number of doublons contains a large number of electronic states. For example, the ground state manifold with no doublons contains

$$\#(\hat{\mathcal{P}}_0^D) = 2^N \binom{L}{N} \quad (12)$$

states for a system with $N \leq L$ electrons.

The preceding definitions for \hat{H}_{FH} and \hat{P} allow us to write the total Hamiltonian of the hybrid system in Fig. 1 as

$$\hat{H} = \hat{H}_{\text{FH}} + \hat{P} + \hat{V}, \quad (13)$$

where \hat{V} accounts for the electron-photon interaction. In Appendix A we outline the derivation of this interaction term from first principles and find

$$\hat{V} = g(\hat{a} + \hat{a}^\dagger) \hat{\mathcal{J}}, \quad (14)$$

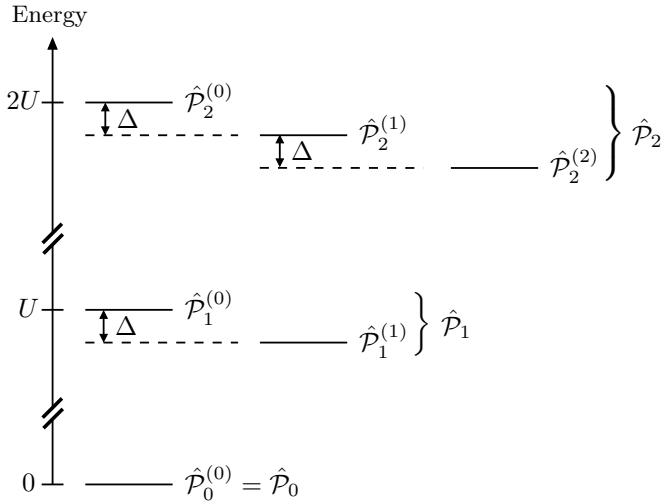


FIG. 2. Schematic drawing of the spectrum of $\hat{H}_0 = \hat{D} + \hat{P}$. $\Delta = \Omega - U$ is the difference between the photon and doublon energies, $\hat{\mathcal{P}}_n^{(j)}$ projects onto a sub-manifold with j photons and $n - j$ doublons, and $\hat{\mathcal{P}}_n = \sum_{j=0}^n \hat{\mathcal{P}}_n^{(j)}$. Higher excitations not shown.

where

$$\hat{\mathcal{J}} = -i \sum_{\langle jk \rangle \sigma} \left(\hat{c}_{j,\sigma}^\dagger \hat{c}_{k,\sigma} - \hat{c}_{k,\sigma}^\dagger \hat{c}_{j,\sigma} \right) \quad (15)$$

is the dimensionless current operator. The parameter $g = t\eta$ in \hat{V} determines the coupling strength between the electrons and photons, and the dimensionless parameter

$$\eta = \frac{de}{\sqrt{2\hbar\epsilon_0\omega_c v}} \quad (16)$$

depends on the lattice constant d and the cavity mode volume v (e : elementary charge, ϵ_0 : vacuum permittivity, \hbar : reduced Planck's constant). The cavity mode couples to both spin components of the electrons in the same way, and the derivation of \hat{V} assumes $\eta \ll 1$. Furthermore, we point out that \hat{V} in Eq. (14) is fundamentally different from cold atom systems where the light-matter coupling is proportional to the atomic density rather than the current.

B. Gross energy structure of \hat{H}

Throughout this work we assume that the photon energy Ω is of the same order of magnitude as the interaction energy U of doubly occupied sites. Since we assume a strongly correlated electron system with $U \gg t$ and since the electron-photon coupling obeys $t \gg g$, we have $U, \Omega \gg t, g$. This separation of energy scales suggests writing the Hamiltonian in Eq. (13) as $\hat{H} = \hat{H}_0 + \hat{H}_1$, where

$$\hat{H}_0 = \hat{D} + \hat{P} \quad (17)$$

describes the energy of doublons and photons, and

$$\hat{H}_1 = \hat{T} + \hat{V} \quad (18)$$

accounts for the kinetic energy and the electron-photon interaction.

Next we investigate the spectrum of \hat{H}_0 in more detail. Due to the structure of \hat{H}_0 its eigenstates $|\mathbf{x}, \mathbf{s}\rangle \otimes |j_P\rangle$ are the tensor product of eigenstates of \hat{D} and \hat{P} . The energies of the states $|\mathbf{x}, \mathbf{s}\rangle$ and $|j_P\rangle$ are determined by their number of doublons and photons, respectively. Here we group the eigenstates of \hat{H}_0 into manifolds with the same number of excitations as shown in Fig. 2, where an excitation can be either a photon or a doublon. There are $n + 1$ possibilities to form n excitations out of doublons and photons, and these decompositions have energies

$$E_n^{(j)} = (n - j)U + j\Omega = nU + j\Delta, \quad (19)$$

where $\Delta = \Omega - U$ is the energy difference between the cavity and the doublon transition, $j \in \{0, \dots, n\}$ denotes the number of photons and $n - j$ is the number of doublons. The corresponding projector onto the sub-manifold with energy $E_n^{(j)}$ is

$$\hat{\mathcal{P}}_n^{(j)} = \hat{\mathcal{P}}_{n-j}^D \otimes \hat{\mathcal{P}}_j^P, \quad (20)$$

where $\hat{\mathcal{P}}_k^D$ and $\hat{\mathcal{P}}_j^P$ are defined in Eqs. (9) and (3), respectively. Finally, we introduce

$$\hat{\mathcal{P}}_n = \sum_{i=0}^n \hat{\mathcal{P}}_n^{(i)}, \quad (21)$$

which is the projector onto the manifold with n excitations.

III. RESULTS

In Sec. II we have shown that the Hamiltonian describing the system in Fig. 1 can be split in two terms that correspond to different energy scales of the problem. The first, large energy scale is given by the electron-electron interaction and the cavity frequency. The second, small energy scale is the hopping amplitude and the electron-cavity coupling. Due to this separation of energy scales we can investigate the physics of the low-energy sector of the system in an effective Hamiltonian approach described in Sec. III A. Results of a numerical investigation of the ground state of this effective Hamiltonian are presented in Sec. III B.

A. Effective Hamiltonian

Here we investigate the physics of the electron-photon coupling in the low-energy manifold \mathcal{P}_0 with zero excitations. The effective Hamiltonian in this ground-state manifold and in second-order perturbation theory

is given by [47]

$$\hat{H}_{\text{gs}} = \hat{\mathcal{P}}_0 \hat{H}_1 \hat{\mathcal{P}}_0 + \sum_{m \neq 0} \sum_{j=0}^m \frac{\hat{\mathcal{P}}_0 \hat{H}_1 \hat{\mathcal{P}}_m^{(j)} \hat{H}_1 \hat{\mathcal{P}}_0}{E_0 - E_m^{(j)}}, \quad (22)$$

where \hat{H}_1 , $E_m^{(j)}$ and $\hat{\mathcal{P}}_m^{(j)}$ are defined in Eqs. (18), (19) and (20), respectively. E_0 is the energy of states in the $\hat{\mathcal{P}}_0$ manifold with respect to \hat{H}_0 , and we set $E_0 = 0$ in the following.

In order to clearly single out the effect of the cavity on the electronic system, we begin with a discussion of the case where the electron-photon coupling is zero, i.e., $g = 0$. In this case only the $m = 0, j = 0$ term contributes in the sum in Eq. (22), and \hat{H}_{gs} reduces to the well-known $tJ\alpha$ model [40],

$$\hat{H}[tJ\alpha] = \hat{\mathcal{P}}_0 (\hat{T} + \hat{H}_{\text{mag}}[J] + \hat{H}_{\text{pair}}[\alpha J]) \hat{\mathcal{P}}_0, \quad (23)$$

where

$$\hat{H}_{\text{mag}}[J] = -J \sum_{\langle kl \rangle} \hat{b}_{kl}^\dagger \hat{b}_{kl}, \quad (24a)$$

$$\hat{H}_{\text{pair}}[\alpha J] = -\alpha J \sum_{\langle\langle klj \rangle\rangle} (\hat{b}_{kl}^\dagger \hat{b}_{lj} + \text{h.c.}), \quad (24b)$$

and

$$\hat{b}_{kl}^\dagger = (\hat{c}_{k,\uparrow}^\dagger \hat{c}_{l,\downarrow}^\dagger - \hat{c}_{k,\downarrow}^\dagger \hat{c}_{l,\uparrow}^\dagger) / \sqrt{2} \quad (25)$$

creates a singlet pair at sites k and l . The physical processes of the $tJ\alpha$ model are illustrated in Fig. 3(b). \hat{T} describes the hopping between adjacent sites, and \hat{H}_{mag} binds nearest-neighbour singlet pairs with energy $J = 4t^2/U$ via superexchange processes. \hat{H}_{pair} describes the hopping of singlet pairs on neighbouring sites as shown in Fig. 3(b), and the sum in Eq. (24b) runs over adjacent sites $\langle\langle klj \rangle\rangle$ with $k < l < j$. The hopping amplitude for singlet pairs is αJ with $\alpha = 1/2$.

The presence of the cavity modifies the effective Hamiltonian in the manifold of zero excitations. The electron-photon interaction \hat{V} couples $\hat{\mathcal{P}}_0$ to the $\hat{\mathcal{P}}_1$ and $\hat{\mathcal{P}}_2$ manifolds and the effective Hamiltonian is [see Appendix B]

$$\hat{H}_{\text{gs}} = \hat{H}[tJ_c \alpha_c] + \hat{\mathcal{P}}_0 (\hat{H}_{\text{shift}} + \hat{H}_{2\text{-site}} + \hat{H}_{\text{long}}) \hat{\mathcal{P}}_0. \quad (26)$$

A comparison with the $tJ\alpha$ model shows that the cavity changes the parameters J and α as shown in Fig. 3(c). We find

$$J_c = J(1 + \mathcal{C}), \quad (27a)$$

$$\alpha_c = \alpha \frac{1 - \mathcal{C}}{1 + \mathcal{C}}, \quad (27b)$$

where

$$\mathcal{C} = \frac{g^2}{t^2} \frac{U}{U + \Omega}. \quad (28)$$

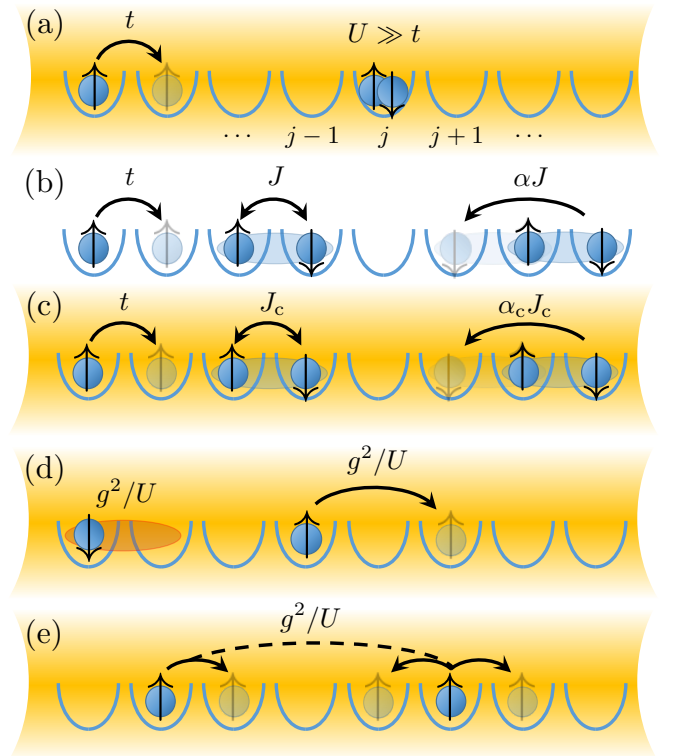


FIG. 3. (Color online) (a) Electronic system coupled to a single-mode cavity. The electronic system is described by a one-dimensional Fermi-Hubbard model with on-site interaction U and hopping amplitude t . (b) Processes in the $tJ\alpha$ model without the cavity where J is the magnetic interaction and αJ is the pair hopping amplitude. (c) The cavity leaves the hopping amplitude t unchanged but gives rise to renormalized parameters J_c and α_c . (d) The cavity introduces a particle-hole binding and enables a next-nearest neighbour hopping term, and (e) enables a long-range electron-electron interaction.

Since $\mathcal{C} > 0$ for $g \neq 0$, the electron-photon interaction increases the magnetic interaction energy J_c , decreases α_c and reduces the pair hopping amplitude

$$\alpha_c J_c = \alpha J (1 - \mathcal{C}) \quad (29)$$

for all parameters $\Omega, U \gg t, g$. Note that J_c is the largest for the smallest Ω compatible with $\Omega \gg t, g$.

In addition, the presence of the cavity results in three additional terms in Eq. (26),

$$\hat{H}_{\text{shift}} = -\frac{g^2}{\Omega} \sum_j [\hat{n}_j (\mathbb{1} - \hat{n}_{j+1}) + \hat{n}_{j+1} (\mathbb{1} - \hat{n}_j)], \quad (30a)$$

$$\hat{H}_{2\text{-site}} = \frac{g^2}{\Omega} \sum_{j\sigma} [(\mathbb{1} - \hat{n}_j) c_{j-1,\sigma}^\dagger c_{j+1,\sigma} + \text{h.c.}], \quad (30b)$$

$$\hat{H}_{\text{long}} = \frac{g^2}{\Omega} \sum_{\substack{k \neq l, l-1 \\ \sigma, \nu}} [\hat{c}_{k,\sigma}^\dagger \hat{c}_{k+1,\sigma} (\hat{c}_{l,\nu}^\dagger \hat{c}_{l+1,\nu} - \hat{c}_{l+1,\nu}^\dagger \hat{c}_{l,\nu}) + \text{h.c.}], \quad (30c)$$

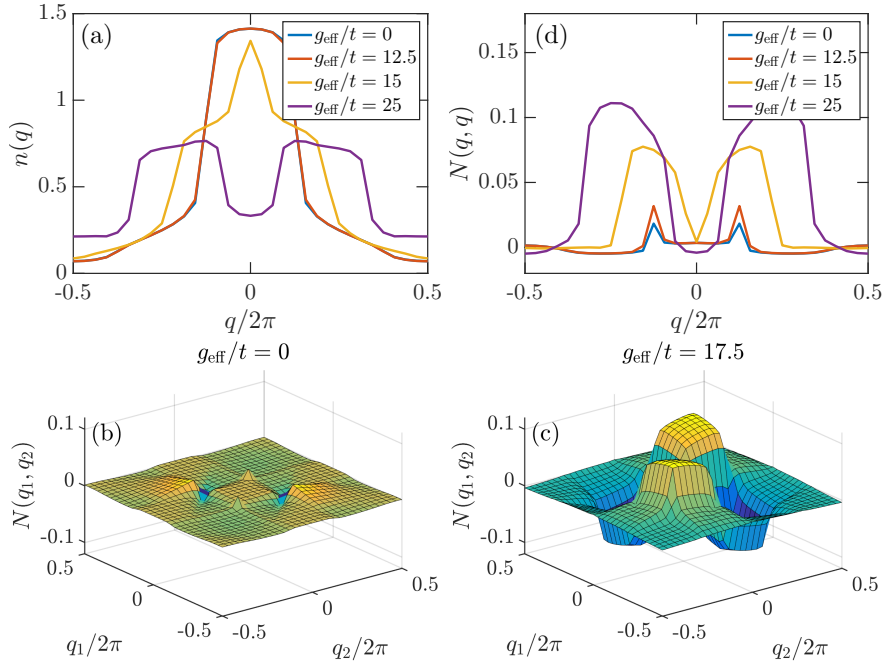


FIG. 4. (Color online) Illustration of the cavity-induced momentum correlations in the system. The model parameters are $U = \Omega = 20t$. The bond dimension used is $\chi = 400$, and the number of sites is $L = 32$, and the system is at quarter-filling $N = 16$ electrons. (a) The momentum distribution of electrons $n(q)$ in the ground state at various values of the cavity coupling g_{eff} . (b) The momentum correlation $N(q_1, q_2)$ with a cavity coupling $g_{\text{eff}}/t = 0$. (c) As in (b), but with a cavity coupling $g_{\text{eff}}/t = 17.5$ after the transition point. (d) A diagonal slice $N(q, q)$ of the momentum correlations highlighting the qualitative difference before and after the transition point.

where $\hat{n}_j = \sum_{\sigma} \hat{n}_{j,\sigma}$. The physical processes induced by \hat{H}_{shift} , $\hat{H}_{2\text{-site}}$ and \hat{H}_{long} are shown in Figs. 3(d) and (e). \hat{H}_{shift} describes an energy shift of all singly-occupied sites with an empty neighbouring site. This effective particle-hole binding energy results from virtual transitions to the empty site and are accompanied by the emission and re-absorption of virtual cavity photons. $\hat{H}_{2\text{-site}}$ accounts for a next-nearest neighbour hopping process and \hat{H}_{long} describes a long-range electron-electron interaction mediated by the cavity. These interactions are independent of the distance between electrons.

We note that this technique of deriving an effective Hamiltonian is similarly applicable to classical driving fields analysed using Floquet theory [41, 42, 48]. In a Floquet context, the zero-excitation sector is coupled to an infinite number of excited sectors $\hat{\mathcal{P}}_m$ with $-\infty \leq m \leq \infty$, representing absorption or emission of m quanta from the driving field. However, the terms in the $+m$ and $-m$ sectors which contribute to \hat{H}_{shift} , $\hat{H}_{2\text{-site}}$ and \hat{H}_{long} exactly cancel in the case of a classical driving field. We conclude that as these terms do not appear for a classical driving field, they are quantum mechanical in origin.

Finally, we note that we have carried out exact diagonalization calculations which confirm the accuracy of the effective Hamiltonian \hat{H}_{gs} in Eq. (26) in the parameter

regime $\Omega, U \gg t, g$, see Appendix B for details.

B. Ground state properties

In order to determine the ground state of the combined electron-photon system we distinguish between electronic systems at half filling and below half filling.

In the case of half filling the effective Hamiltonian in Eq. (26) reduces to $\hat{H}_{\text{gs}} = \hat{\mathcal{P}}_0 \hat{H}_{\text{mag}}[J_c] \hat{\mathcal{P}}_0$. This is the Hamiltonian of the $tJ\alpha$ model at half filling, i.e. an isotropic Heisenberg model with coupling J_c . The ground state of \hat{H}_{gs} is thus an antiferromagnetic state [40] with increased exchange interaction $J_c > J$ due to the electron-photon coupling.

To investigate the ground state at less than half filling, we perform finite-system DMRG calculations as implemented in the open source Tensor Network Theory (TNT) library [46]. The matrix product operator corresponding to the Hamiltonian H_{gs} is built using the finite automata technique [49, 50]. We use a maximum matrix product state bond dimension of $\chi = 400$, resulting in a typical truncation error per bond of $\sim 10^{-4}$.

The most important term in the Hamiltonian determining the structure of the ground state is \hat{H}_{long} . Due to the infinite-range of the interaction, its total energy con-

tribution dominates that of the strictly nearest-neighbour terms, scaling with $\sim L^2$ rather than $\sim L$. To account for this expected length-dependence of the coupling term, we define an effective cavity coupling

$$g_{\text{eff}} = 4g\sqrt{L \ln 2} \approx 3.33g\sqrt{L}. \quad (31)$$

To explore the effect of the cavity terms, we first compute the momentum distribution of electrons in the ground state,

$$n(q) = \langle \sum_{\sigma} \hat{c}_{q,\sigma}^{\dagger} \hat{c}_{q,\sigma} \rangle, \quad (32)$$

where $\hat{c}_{q,\sigma} = \sum_j e^{-ijq} \hat{c}_{j,\sigma} / \sqrt{L}$. As shown in Fig. 4(a), when $g_{\text{eff}}/t = 0$ (i.e. the bare $tJ\alpha$ model), a distorted Fermi surface with the electrons centered about $q = 0$ is seen. When the cavity coupling is switched to sufficiently large values $g_{\text{eff}}/t \gtrsim 15$, the Fermi surface splits into two smaller peaks at finite momenta. We find that when plotted as a function of the rescaled g_{eff} , the transition occurs at the same value *independent* of the system size L , as expected.

Further information is revealed by looking at the momentum-space electron correlations,

$$N(q_1, q_2) = \langle c_{q_1,\uparrow}^{\dagger} c_{q_1,\uparrow} c_{q_2,\downarrow}^{\dagger} c_{q_2,\downarrow} \rangle \quad (33)$$

which is shown in Fig. 4(b) and Fig. 4(c) for $g_{\text{eff}}/t = 0$ and $g_{\text{eff}}/t = 17.5$ respectively. We find that the cavity induced \hat{H}_{long} terms induce momentum-space pairing correlations such that pairs of ‘‘up’’ and ‘‘down’’ electrons always move in the same direction. In Fig. 4(d) we show diagonal cuts $N(q, q)$ at various values of g_{eff} , highlighting the induced correlations.

In addition to $n(q)$ and $N(q_1, q_2)$ we calculated spin-spin correlations [51] and find that they are approximately unchanged after the transition. This is because although J_c and α_c are substantially modified by the presence of the cavity, they still lie below the required threshold to induce a magnetic phase transition [51]. The more important term, \hat{H}_{long} is spin agnostic, acting only on the charge degree of freedom.

IV. EXPERIMENTAL REALIZATION

Next we discuss the experimental observation of the predicted effects. The change in the magnetic interaction energy in the ground state at half filling could, e.g., be observed by measuring changes in the magnetic susceptibility $\Delta\chi \propto \Delta J \propto \eta^2$ of the material [52]. In order to predict the magnitude of this effect mediated by the exchange of virtual photons, we consider ET-F₂TCNQ [53, 54] which is a generic example of a one-dimensional Mott insulator where $U \gg t$. A cavity mode with wavelength $\lambda_c \approx 1.8\mu\text{m}$ corresponding to the Mott gap $U \approx 0.7\text{eV}$ in ET-F₂TCNQ results in $\eta \approx 3 \times 10^{-5} \sqrt{\lambda_c^3/v}$. This shows that significant coupling

strengths require nanoplasmonic cavities [55] where small values of v/λ_c^3 can be achieved. In order to change J by $\approx 1\%$, we require $v/\lambda_c^3 \lesssim 10^{-7}$. Such small cavity volumes have been experimentally achieved recently [55] for wavelengths in the THz regime. Similarly small volumes for higher frequencies are expected to be available in the near future, e.g., by using superconducting cavities [56, 57].

In order to observe the cavity-induced pairing in momentum space at less than half filling we require $g_{\text{eff}}/t \gtrsim 15$. If the material fills the mode volume of the cavity, g_{eff} just depends on the volume per lattice site v_{uc} . Nanoplasmonic cavities are thus not required to observe the momentum-space pairing effect. In the case of ET-F₂TCNQ we find $g_{\text{eff}}/t \approx 6.4$. While this value is too small by about a factor of two in order to observe the new phase, larger values of g_{eff}/t are possible in materials with a smaller Mott gap or smaller unit cells.

V. SUMMARY AND DISCUSSION

In summary, we have shown that second-order electron-photon interactions enhance superexchange interactions giving rise to the antiferromagnetic ground state of the one-dimensional Fermi-Hubbard model at half filling.

Moreover, we have shown that at sufficiently large couplings, the cavity induces fermion-pairing in momentum space. In higher dimensions we speculate that this could lead to cavity-induced superconductivity [28]. Such effects do not emerge from a Floquet analysis of a classical light field, and so are genuinely quantum mechanical in nature. Similarly, substantial modification of the superexchange J can only be achieved by classical light fields when they are extremely intense [41–43]. Here this is achieved by strong coupling to an empty cavity.

Finally, we note that our results are directly applicable to higher-dimensional electronic systems where the electron-cavity interaction can be tuned via the relative orientation between the crystal and the cavity polarization vector, see Appendix A. The rich physics ensuing from this anisotropic interaction is subject to future studies.

ACKNOWLEDGMENTS

MK and DJ acknowledge financial support from the National Research Foundation and the Ministry of Education, Singapore. DJ and FS acknowledge funding from the European Research Council under the European Union’s Seventh Framework Programme (FP7/2007-2013)/ERC Grant Agreement no. 319286, Q-MAC.

Appendix A: Electron-Photon interaction

The Hubbard Hamiltonian \hat{H}_{FH} and the cavity Hamiltonian \hat{P} are defined in Eqs. (4) and (1), respectively. Interactions between the two sub-systems can be accounted for via the Peierls substitution [40] $\hat{T} \rightarrow \hat{T}_{\text{PS}}$, where

$$\hat{T}_{\text{PS}} = -t \sum_{(jk)\sigma} \left(\hat{c}_{j,\sigma}^\dagger \hat{c}_{k,\sigma} e^{i\frac{e}{\hbar} \int_{r_j}^{r_k} \hat{\mathbf{A}}(\mathbf{r}') \cdot d\mathbf{r}'} + \text{h.c.} \right), \quad (\text{A1})$$

\mathbf{r}_i is the position vector of site i and

$$\hat{\mathbf{A}} = A_0(a + a^\dagger)\mathbf{u} \quad (\text{A2})$$

is the quantized vector potential of the cavity field in Coulomb gauge. In Eq. (A2) \mathbf{u} is the mode function of the cavity field,

$$A_0 = \sqrt{\frac{\hbar}{2\varepsilon_0\omega_c v}}, \quad (\text{A3})$$

ε_0 is the vacuum permittivity and v is the mode volume. In the following we neglect the position dependence of the mode function and assume that $\mathbf{u} = \mathbf{e}_c$, where \mathbf{e}_c is the unit polarization vector of the cavity field. Assuming that \mathbf{e}_c is aligned with the direction of the atomic chain we obtain

$$\hat{T}_{\text{PS}} = -t \sum_{(jk)\sigma} \left(\hat{c}_{j,\sigma}^\dagger \hat{c}_{k,\sigma} e^{i\eta(\hat{a} + \hat{a}^\dagger)} + \text{h.c.} \right), \quad (\text{A4})$$

where the dimensionless parameter η is defined in Eq. (16) and $d = |\mathbf{r}_{j+1} - \mathbf{r}_j|$ is the lattice constant. The full Hamiltonian of the hybrid system comprising the electrons, photons and their interactions is thus

$$\hat{H}_{\text{hybrid}} = \hat{T}_{\text{PS}} + \hat{P} + \hat{D}. \quad (\text{A5})$$

Expanding Eq. (A4) up to first order in η for $\eta \ll 1$ results in

$$\hat{T}_{\text{PS}} \approx \hat{T} + \hat{V}, \quad (\text{A6})$$

where \hat{V} is defined in Eq. (14). is the dimensionless current operator. For $\eta \ll 1$, $\hat{H}_{\text{hybrid}} \approx \hat{H} = \hat{H}_{\text{FH}} + \hat{P} + \hat{V}$ is thus well approximated by the system Hamiltonian \hat{H} defined in Eq. (13).

The generalization of the electron-photon interaction to higher-dimensional electronic systems is straightforward. In particular, for a three-dimensional crystal whose unit cell is described by the lattice vectors \mathbf{d}_α we obtain

$$\hat{V}_{\text{3D}} = (\hat{a} + \hat{a}^\dagger) \frac{e}{\sqrt{2\hbar\varepsilon_0\omega_c v}} \sum_\alpha t_\alpha (\mathbf{e}_c \cdot \mathbf{d}_\alpha) \hat{\mathcal{J}}_\alpha, \quad (\text{A7})$$

where t_α and $\hat{\mathcal{J}}_\alpha$ are the hopping amplitude and the current operator in the direction of \mathbf{d}_α , respectively. It follows that the electron-cavity coupling depends on the relative orientation between the crystal and the cavity field. Note that we did not employ the rotating-wave approximation in Eqs. (14) and (A7). As a matter of fact, the counter-rotating terms give rise to the dominant contribution to the cavity-mediated effects in the ground state manifold.

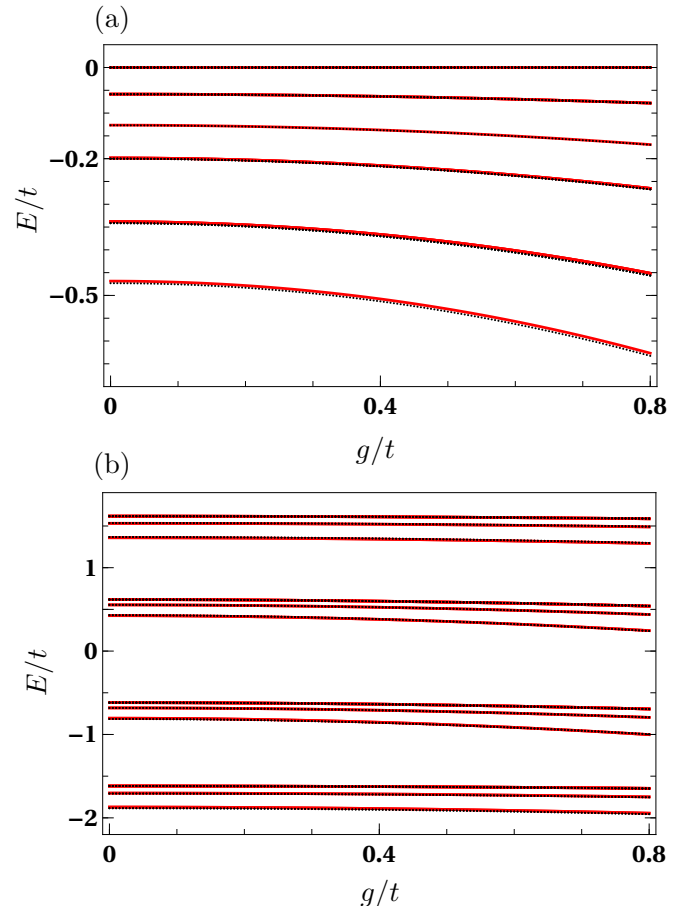


FIG. 5. (Color online) Comparison of the eigenenergies E of the system Hamiltonian \hat{H} in Eq. (13) in the ground state manifold and the effective Hamiltonian \hat{H}_{gs} in Eq. (26) for a system with $L = 4$ sites as a function of the cavity coupling g . The eigenvalues corresponding to \hat{H} (\hat{H}_{gs}) are shown by red solid (black dotted) lines. The exact diagonalization calculations take into account photon states $|j_P\rangle$ with $j \in \{0, 1, 2\}$. (a) Half filling with $N = 4$ electrons and $U = 20t$ and $\Omega = 18t$. (b) Same as in (a) but for $N = 3$ electrons.

Appendix B: Evaluation of H_{gs}

The first term in Eq. (22) reduces to $\hat{\mathcal{P}}_0 \hat{T} \hat{\mathcal{P}}_0$ since $\hat{\mathcal{P}}_0 \hat{V} \hat{\mathcal{P}}_0 = 0$, i.e., the first-order contribution of the electron-photon coupling to \hat{H}_{gs} vanishes. The sum in Eq. (22) accounts for all second-order processes, and only the three terms with indices $(m = 1, j = 0)$, $(m = 2, j = 1)$ and $(m = 1, j = 1)$ make a non-zero contribution to this sum. $(m = 1, j = 0)$ corresponds to the standard $tJ\alpha$ model, and $(m = 2, j = 1)$ and $(m = 1, j = 1)$ account for the modifications due to the cavity. In the following we discuss these three contributions in more detail:

- $(m = 1, j = 0)$: This term corresponds to processes where one doublon is created and subsequently annihilated. These processes only involve the hopping term \hat{T}

and are independent of the electron-photon interaction \hat{V} ,

$$\begin{aligned} -\frac{1}{U}\hat{\mathcal{P}}_0\hat{H}_1\hat{\mathcal{P}}_1^{(0)}\hat{H}_1\hat{\mathcal{P}}_0 &= -\frac{1}{U}[\hat{\mathcal{P}}_0^D\hat{T}\hat{\mathcal{P}}_1^D\hat{T}\hat{\mathcal{P}}_0^D]\otimes\hat{\mathcal{P}}_0^P \\ &= \hat{\mathcal{P}}_0(\hat{H}_{\text{mag}}[J] + \hat{H}_{\text{pair}}[\alpha J])\hat{\mathcal{P}}_0, \end{aligned} \quad (\text{B1})$$

where $\hat{H}_{\text{mag}}[J]$ and $\hat{H}_{\text{pair}}[\alpha J]$ are defined in Eqs. (24a) and (24b), respectively, $J = 4t^2/U$ and $\alpha = 1/2$.

- ($m = 2, j = 1$): This term accounts for the virtual creation and subsequent annihilation of one photon and one doublon,

$$\begin{aligned} -\frac{1}{\Omega + U}\hat{\mathcal{P}}_0\hat{H}_1\hat{\mathcal{P}}_2^{(1)}\hat{H}_1\hat{\mathcal{P}}_0 &= -\frac{g^2}{\Omega + U}[\hat{\mathcal{P}}_0^D\hat{J}\hat{\mathcal{P}}_1^D\hat{J}\hat{\mathcal{P}}_0^D]\otimes\hat{\mathcal{P}}_0^P \\ &= \hat{\mathcal{P}}_0\left(\hat{H}_{\text{mag}}\left[\frac{4g^2}{U + \Omega}\right] + \hat{H}_{\text{pair}}\left[-\frac{2g^2}{U + \Omega}\right]\right)\hat{\mathcal{P}}_0. \end{aligned} \quad (\text{B2})$$

The terms in Eq. (B2) result in a re-normalization of the magnetic exchange energy and the pair hopping of the $tJ\alpha$ model.

- ($m = 1, j = 1$): This term describes processes where an electron hops to a neighbouring empty site and a photon is emitted, followed by the re-absorption of the photon and a second hopping process. We find

$$\begin{aligned} -\frac{1}{\Omega}\hat{\mathcal{P}}_0\hat{H}_1\hat{\mathcal{P}}_1^{(1)}\hat{H}_1\hat{\mathcal{P}}_0 &= -\frac{g^2}{\Omega}[\hat{\mathcal{P}}_0^D\hat{J}\hat{\mathcal{P}}_0^D\hat{J}\hat{\mathcal{P}}_0^D]\otimes\hat{\mathcal{P}}_0^P \\ &= \hat{\mathcal{P}}_0(\hat{H}_{\text{shift}} + \hat{H}_{2\text{-site}} + \hat{H}_{\text{long}})\hat{\mathcal{P}}_0, \end{aligned} \quad (\text{B3})$$

where \hat{H}_{shift} , $\hat{H}_{2\text{-site}}$ and \hat{H}_{long} are defined in Eq. (30). Each process in Eq. (B3) involves two electron hops

without creating a doublon. Depending on whether the two hopping processes go in the same or opposite direction, one obtains a particle-hole binding effect (\hat{H}_{shift}) or a next-nearest neighbour tunneling term ($\hat{H}_{2\text{-site}}$). The virtual photon can even be emitted and absorbed by two different electrons, which gives rise to the cavity-mediated long-range interaction \hat{H}_{long} . Note that all terms in Eq. (B3) are zero at half filling, since in this case electron hops without creating a doublon are impossible.

Combining all terms in Eqs.(B1), (B2) and (B3) gives \hat{H}_{gs} in Eq. (26). In order to test the accuracy of this effective Hamiltonian, we compare its spectrum to the eigenvalues of the system Hamiltonian in Eq. (13) via exact diagonalization. We find that the eigenvalues of the two Hamiltonians are in excellent agreement for sufficiently large values of U and Ω , and for a wide range of coupling strengths g . More specifically, the differences between the eigenvalues are of the order of $t^4/[\min(U, \Omega)]^2$, which is the magnitude of the next higher-order terms in the perturbation series. We present two examples of these calculations for a system with $L = 4$ sites in Fig. 5, where Fig. 5(a) and Fig. 5(b) correspond to half filling ($N = 4$ electrons) and less than half filling ($N = 3$ electrons), respectively. Note that we chose a small system and an unrealistically large range of the cavity coupling parameter g for illustration purposes. Finally, we point out that some of the eigenvalues shown in Fig. 5 are degenerate. The total number of states in Figs. 5(a) and (b) are 16 and 32, respectively.

-
- [1] Z.-L. Xiang, S. Ashhab, J. Q. You, and F. Nori, "Hybrid quantum circuits: Superconducting circuits interacting with other quantum systems," *Rev. Mod. Phys.* **85**, 623 (2013).
- [2] G. Kurizki, P. Bertet, Y. Kubo, K. Mølmer, D. Petrosyan, P. Rabl, and J. Schmiedmayer, "Quantum technologies with hybrid systems," *PNAS* **112**, 3866 (2015).
- [3] P. Domokos and H. Ritsch, "Collective cooling and self-organization of atoms in a cavity," *Phys. Rev. Lett.* **89**, 253003 (2002).
- [4] D. Nagy, G. Szirmai, and P. Domokos, "Self-organization of a Bose-Einstein condensate in an optical cavity," *Eur. Phys. J. D* **48**, 127 (2008).
- [5] A. T. Black, H. W. Chan, and V. Vuletić, "Observation of collective friction forces due to spatial self-organization of atoms: From Rayleigh to Bragg scattering," *Phys. Rev. Lett.* **91**, 203001 (2003).
- [6] H. Ritsch, P. Domokos, F. Brennecke, and T. Esslinger, "Cold atoms in cavity-generated dynamical optical potentials," *Rev. Mod. Phys.* **85**, 553 (2013).
- [7] F. Piazza, P. Strack, and W. Zwerger, "Bose-Einstein condensation versus Dicke-Hepp-Lieb transition in an optical cavity," *Ann. Phys.* **339**, 135 (2013).
- [8] D. Jaksch, S. A. Gardiner, K. Schulze, J. I. Cirac, and P. Zoller, "Uniting Bose-Einstein condensates in optical resonators," *Phys. Rev. Lett.* **86**, 4733 (2001).
- [9] K. Baumann, C. Guerlin, F. Brennecke, and T. Esslinger, "Dicke quantum phase transition with a superfluid gas in an optical cavity," *Nature* **464**, 1301 (2010).
- [10] R. Landig, L. Hruby, N. Dogra, M. Landini, R. Mottl, T. Donner, and T. Esslinger, "Quantum phases from competing short- and long-range interactions in an optical lattice," *Nature* **532**, 476 (2016).
- [11] C. Kollath, A. Sheikhan, S. Wolff, and F. Brennecke, "Ultracold fermions in a cavity-induced artificial magnetic field," *Phys. Rev. Lett.* **116**, 060401 (2016).
- [12] X. Zhang, C.-L. Zou, L. Jiang, and H. X. Tang, "Strongly coupled magnons and cavity microwave photons," *Phys. Rev. Lett.* **113**, 156401 (2014).
- [13] Y. Tabuchi, S. Ishino, T. Ishikawa, R. Yamazaki, K. Usami, and Y. Nakamura, "Hybridizing ferromagnetic magnons and microwave photons in the quantum limit," *Phys. Rev. Lett.* **113**, 083603 (2014).

- [14] B. M. Yao, Y. S. Gui, Y. Xiao, H. Guo, X. S. Chen, W. Lu, C. L. Chien, and C.-M. Hu, “Theory and experiment on cavity magnon-polariton in the one-dimensional configuration,” *Phys. Rev. B* **92**, 184407 (2015).
- [15] P. Sivarajah and J. Lu and M. Xiang and S. Kamba and S. Cao and K. Nelson, *Terahertz-frequency magnon-phonon-polaritons in the strong coupling regime*, arXiv:1611.01814v3 .
- [16] L. V. Abdurakhimov, S. Khan, N. A. Panjwani, J. D. Breeze, S. Seki, Y. Tokura, J. J. L. Morton, and H. Kurebayashi, *Strong coupling between magnons in a chiral magnetic insulator Cu_2OSeO_3 and microwave cavity photons*, arXiv:1802.07113v1.
- [17] M. Mergenthaler, J. Liu, J. J. Le Roy, N. Ares, A. L. Thompson, L. Bogani, F. Luis, S. J. Blundell, T. Lancaster, A. Ardavan, G. A. Briggs, P. J. Leek, and E. A. Laird, “Strong coupling of microwave photons to antiferromagnetic fluctuations in an organic magnet,” *Phys. Rev. Lett.* **119**, 147701 (2017).
- [18] D. Hagenmüller, S. De Liberato, and C. Ciuti, “Ultrastrong coupling between a cavity resonator and the cyclotron transition of a two-dimensional electron gas in the case of an integer filling factor,” *Phys. Rev. B* **81**, 235303 (2010).
- [19] G. Scalari, C. Maissen, D. Turčinková, D. Hagenmüller, S. De Liberato, C. Ciuti, C. Reichl, D. Schuh, W. Wegscheider, M. Beck, and J. Faist, “Ultrastrong coupling of the cyclotron transition of a 2D electron gas to a THz metamaterial,” *Science* **335**, 1323 (2012).
- [20] Q. Zhang, M. Lou, X. Li, J. L. Reno, W. Pan, J. D. Watson, M. J. Manfra, and J. Kono, “Collective non-perturbative coupling of 2D electrons with high-quality-factor terahertz cavity photons,” *Nat. Phys.* **12**, 1005 (2016).
- [21] X. Li, M. Bamba, Q. Zhang, S. Fallahi, G. C. Gardner, W. Gao, M. Lou, K. Yoshioka, M. J. Manfra, and J. Kono, “Vacuum Bloch–Siegert shift in Landau polaritons with ultra-high cooperativity,” *Nat. Photon.* **12**, 324 (2018).
- [22] G. L. Paravicini-Bagliani, F. Appugliese, E. Richter, F. Valmorra, J. Keller, M. Beck, C. Rössler, T. Ihn, K. Ensslin, G. Scalari, and J. Faist, *Tomography of an ultrastrongly coupled polariton state using magneto-transport in the quantum regime*, arXiv:1805.00846v1 (2018).
- [23] N. Bartolo and C. Ciuti, *Vacuum-dressed cavity magnetotransport of a 2D electron gas*, arXiv:1805.02623v1 (2018).
- [24] E. Orgiu, J. George, J. A. Hutchison, E. Devaux, J. F. Dayen, B. Doudin, F. Stellacci, C. Genet, J. Schachenmayer, C. Genes, G. Pupillo, P. Samorí, and T. W. Ebbesen, “Conductivity in organic semiconductors hybridized with the vacuum field,” *Nature Mat.* **14**, 1123 (2015).
- [25] J. Feist and F. J. Garcia-Vidal, “Extraordinary exciton conductance induced by strong coupling,” *Phys. Rev. Lett.* **114**, 196402 (2015).
- [26] J. Schachenmayer, C. Genes, E. Tignone, and G. Pupillo, “Cavity-enhanced transport of excitons,” *Phys. Rev. Lett.* **114**, 196403 (2015).
- [27] Y. Laplace, S. Fernandez-Pena, S. Gariglio, J. M. Triscone, and A. Cavalleri, “Proposed cavity Josephson plasmonics with complex-oxide heterostructures,” *Phys. Rev. B* **93**, 075152 (2016).
- [28] F. Schlawin, A. Cavalleri, and D. Jaksch, *Cavity-mediated electron-photon superconductivity*, arXiv:1804.07142.
- [29] J. B. Curtis and Z. M. Raines and A. A. Allocca and M. Hafezi and V. M. Galitski, *Cavity Quantum Eliashberg Enhancement of Superconductivity*, arXiv:1805:04182v1.
- [30] G. Mazza and A. Georges, “Superradiant quantum materials,” *Phys. Rev. Lett.* **122**, 017401 (2019).
- [31] Editorial, “The rise of quantum materials,” *Nat. Phys.* **12**, 105 (2016).
- [32] B. J. Powell and R. H. McKenzie, “Strong electronic correlations in superconducting organic charge transfer salts,” *J. Phys.: Condens. Matter* **18**, R827 (2006).
- [33] B. J. Powell and R. H. McKenzie, “Quantum frustration in organic Mott insulators: from spin liquids to unconventional superconductors,” *Rep. Prog. Phys.* **74**, 056501 (2011).
- [34] R. Kato, “Conducting metal dithiolene complexes: Structural and electronic properties,” *Chem. Rev.* **104**, 5319 (2004).
- [35] M. A. Sentef and M. Ruggenthaler and A. Rubio, *Cavity quantum- electrodynamical polaritonically enhanced superconductivity*, arXiv:1802.09437.
- [36] D. Fausti, R. I. Tobey, N. Dean, S. Kaiser, A. Dienst, M. C. Hoffmann, S. Pyon, T. Takayama, H. Takagi, and A. Cavalleri, “Light-induced superconductivity in a stripe-ordered cuprate,” *Science* **331**, 189 (2011).
- [37] W. Hu, S. Kaiser, D. Nicoletti, C. R. Hunt, I. Gierz, M. C. Hoffmann, M. Le Tacon, T. Loew, B. Keimer, and A. Cavalleri, “Optically enhanced coherent transport in $YBa_2Cu_3O_{6.5}$ by ultrafast redistribution of interlayer coupling,” *Nature Mater.* **13**, 705 (2014).
- [38] M. Mitrano, A. Cantaluppi, D. Nicoletti, S. Kaiser, A. Perucchi, S. Lupi, P. Di Pietro, D. Pontiroli, M. Riccò, S. R. Clark, D. Jaksch, and A. Cavalleri, “Possible light-induced superconductivity in K_3C_{60} at high temperature,” *Nature* **530**, 461 (2016).
- [39] M. A. Sentef, A. Tokuno, A. Georges, and C. Kollath, “Theory of laser-controlled competing superconducting and charge orders,” *Phys. Rev. Lett.* **118**, 087002 (2017).
- [40] F.H.L. Essler, H. Frahm, F. Göhmann, A. Klümper, and V.E. Korepin, *The One-Dimensional Hubbard Model* (Cambridge University Press, 2005).
- [41] J. Mentink, K. Balzer, and M. Eckstein, “Ultrafast and reversible control of the exchange interaction in Mott insulators,” *Nat. Commun.* **6**, 6708 (2015).
- [42] J. R. Coulthard, S. R. Clark, S. Al-Assam, A. Cavalleri, and D. Jaksch, “Enhancement of superexchange pairing in the periodically driven Hubbard model,” *Phys. Rev. B* **96**, 085104 (2017).
- [43] F. Görg, M. Messer, K. Sandholzer, G. Jotzu, R. Desbuquois, and T. Esslinger, “Enhancement and sign change of magnetic correlations in a driven quantum many-body system,” *Nature* **553**, 481 (2018).
- [44] E. A. Stepanov, C. Dutreix, and M. I. Katsnelson, “Dynamical and reversible control of topological spin textures,” *Phys. Rev. Lett.* **118**, 157201 (2017).
- [45] Ulrich Schollwöck, “The density-matrix renormalization group in the age of matrix product states,” *Annals of Physics* **326**, 96 – 192 (2011).
- [46] S. Al-Assam, S. R. Clark, and D. Jaksch, “The tensor network theory library,” *Journal of Statistical Mechanics: Theory and Experiment* **2017**, 093102 (2017).
- [47] C. Cohen-Tannoudji, J. Dupont-Roc, and G. Grynberg, *Atom-Photon Interactions* (1998).
- [48] A. Eckardt and E. Anisimovas, “High-frequency approx-

- imation for periodically driven quantum systems from a floquet-space perspective,” *New Journal of Physics* **17**, 093039 (2015).
- [49] Gregory M. Crosswhite and Dave Bacon, “Finite automata for caching in matrix product algorithms,” *Physical Review A* **78**, 012356 (2008).
- [50] Sebastian Paeckel, Thomas Köhler, and Salvatore R. Manmana, “Automated construction of $U(1)$ -invariant matrix-product operators from graph representations,” *SciPost Phys.* **3**, 035 (2017).
- [51] J. R. Coulthard, S. R. Clark, and D. Jaksch, “Ground-state phase diagram of the one-dimensional $t-j$ model with pair hopping terms,” *Phys. Rev. B* **98**, 035116 (2018).
- [52] M. Tamura and R. Kato, “Magnetic susceptibility of $\beta' - [\text{Pd}(\text{dmit})_2]$ salts (dmit=1, 3-dithiol-2-thione-4, 5-dithiolate, C_3S_5): evidence for frustration in spin-1/2 heisenberg antiferromagnets on a triangular lattice,” *J. Phys.: Condens. Matter* **14**, L729 (2002).
- [53] T. Hasegawa, S. Kagoshima, T. Mochida, S. Sug-iura, and Y. Iwasa, “Electronic states and anti-ferromagnetic order in mixed-stack charge-transfer compound (BEDT-TTF)(F_2TCNQ),” *Solid State Commun.* **103**, 489 (1997).
- [54] T. Hasegawa, T. Mochida, R. Kondo, S. Kagoshima, Y. Iwasa, T. Akutagawa, T. Nakamura, and G. Saito, “Mixed-stack organic charge-transfer complexes with intercolumnar networks,” *Phys. Rev. B* **62**, 10059 (2000).
- [55] J. Keller, G. Scalari, S. Cibella, C. Maissen, F. Ap-pugliese, E. Giovine, R. Leoni, M. Beck, and J. Faist, “Few-electron ultrastrong light-matter coupling at 300 GHz with nanogap hybrid LC microcavities,” *Nano Lett.* **17**, 7410 (2017).
- [56] G. Scalari, C. Maissen, S. Cibella, R. Leoni, P. Carelli, F. Valmorra, M. Beck, and J. Faist, “Superconducting complementary metasurfaces for THz ultrastrong light-matter coupling,” *New J. Phys.* **16**, 033005 (2014).
- [57] G. Scalari, C. Maissen, S. Cibella, R. Leoni, and J. Faist, “High quality factor, fully switchable terahertz super-conducting metasurface,” *Appl. Phys. Lett.* **105**, 261104 (2014).